

# REAL-TIME MODULATED NANOPARTICLE SEPARATION WITH AN ULTRA-LARGE DYNAMIC RANGE

*Kerwin Kwek Zeming<sup>a</sup>, Nitish V. Thakor<sup>a,b</sup>, Yong Zhang<sup>c,d\*</sup>, Chia-Hung Chen<sup>a,c\*</sup>*

Author affiliation:

*a*: Singapore Institute for Neurotechnology (SINAPSE), 28 Medical Dr. #05-COR, Singapore 117456

*b*: Department of Biomedical Engineering, Johns Hopkins University School of Medicine, Traylor 701 / 720 Rutland Ave, Baltimore, MD 21205

*c*: Department of Biomedical Engineering, National University of Singapore, 9 Engineering Drive 1, Block EA #03-12, Singapore 117576,

*d*: Cellular and Molecular Bioengineering Lab, National University of Singapore, Block E3A, #07-06, 7 Engineering Drive 1, Singapore 117574

\*Corresponding Authors:

Yong Zhang

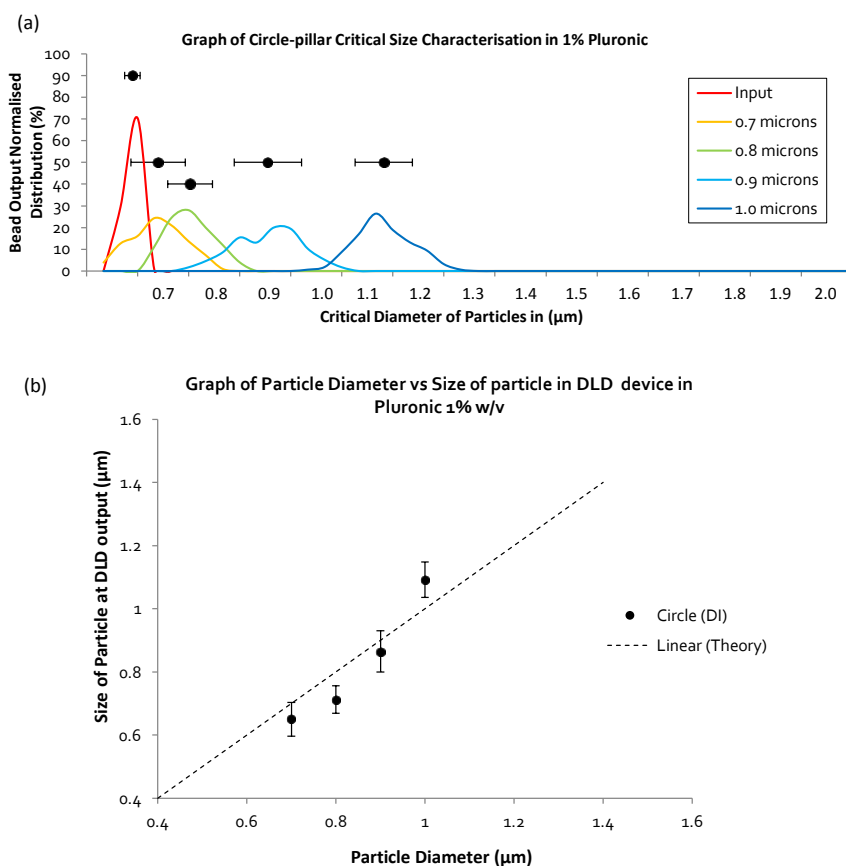
Department of Biomedical Engineering,  
National University of Singapore,  
9 Engineering Drive 1, Block EA #03-12, Singapore 117576  
+65 6516 4871  
[biezy@nus.edu.sg](mailto:biezy@nus.edu.sg)

Chia-Hung Chen

Department of Biomedical Engineering,  
National University of Singapore,  
9 Engineering Drive 1, Block EA #03-12, Singapore 117576  
+65 98514596  
[biecch@nus.edu.sg](mailto:biecch@nus.edu.sg)

## Supplementary Information 1: DLD Device calibration

1% (w/v) pluronic F127 solution was used to pre-treat the device to prevent non-specific binding of beads onto the surface of the device. Similar to previous works, we tested the bead separation in pluronic solution to reduce any adsorption of beads during the experiment which may clog up the device.<sup>1,2</sup> The separation spectrum of NIST polystyrene beads ranging from 0.7  $\mu\text{m}$  to 1.0  $\mu\text{m}$  is shown in Supplementary Figure-S2a. Based on the empirical model ( $D_c = 1.4g\varepsilon^{0.48}$ ), a 1.0  $\mu\text{m}$  polystyrene bead should be laterally displaced and exhibit a DLD output particle size of 1.0  $\mu\text{m}$ . The mean bead separation size can be approximated with the DLD empirical model depicted by the dotted line in Fig-S2(b). Hence the separation of bead sizes agrees with the DLD model in a 1%(w/v) pluronic F127 solution.



**Supplementary Figure-S1: Particle bead separation in 1% pluronic F127 (w/v) solution.** (a) shows the spectral distribution of 0.7  $\mu\text{m}$ , 0.8  $\mu\text{m}$ , 0.9  $\mu\text{m}$  and 1.0  $\mu\text{m}$  beads at the output of the DLD device in pluronic F127 solution. The mean apparent particle size is plot in comparison with the actual size of the beads in (b).

Using this calibration method, it would naturally seem that  $D_{\text{app}} = D_p$  and  $d_{\text{F-EDL}}$  is non-existent. However, the surfactant concentration used is at such high concentrations such that the dipole interactions of the surfactant pluronic F127 cannot be ignored. This is also the reason why previously we did not observe any effects based on the ionic concentration of the colloidal systems.

## Supplementary Information 2: Debye length calculations and discussion

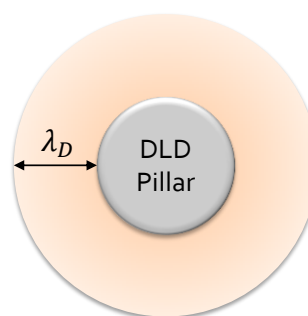
Debye length of a monovalent ionic solution can be calculated in the following formula:

$$\lambda_D = \sqrt{\frac{\epsilon_r \epsilon_0 k_b T}{2 N_A e^2 I}} \quad (1)$$

Where  $\epsilon_r$  is the electric permittivity of the fluid,  $\epsilon_0$  is the electric permittivity of free space,  $k_b$  is the Boltzmann constant,  $T$  is the temperature in kelvins,  $N_A$  is Avogadro's constant,  $e$  is the elementary charge and  $I$  is the ionic concentration of the ions. Increasing ionic concentration would reduce the Debye length as shown in Fig-S1. The selected Debye lengths to be tested correspond to the respective ionic concentrations.

NaCl Concentrations $I$ ( $\mu\text{M}$ )	Debye Length $\lambda_D$ (nm)
$\sim 0.1$ (DI water [ $\text{H}^+$ ] ions conc.)	970
10	97
16	75
37	50
75	35
150	25
500	12.5
$\sim 100000$ (PBS concentration)	$\sim 1$

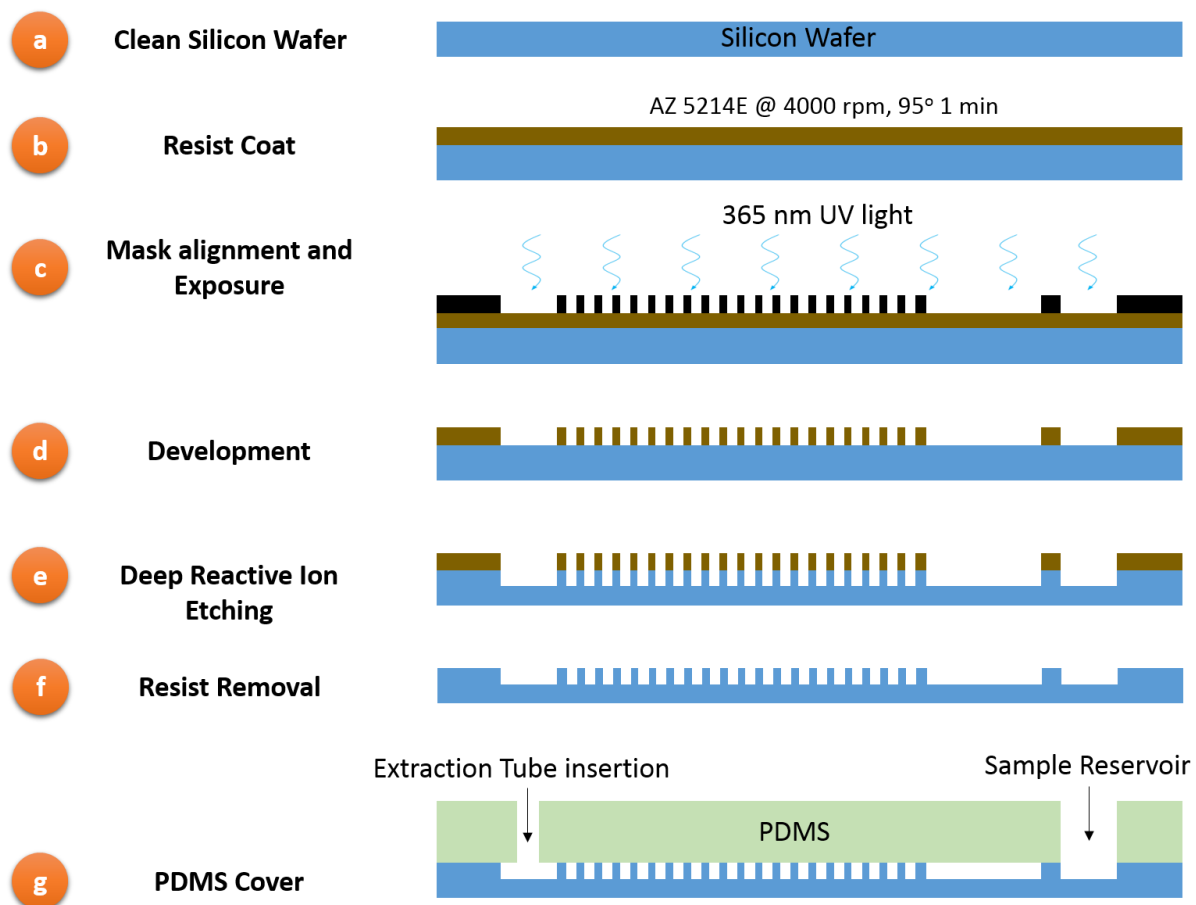
$$\lambda_D = \sqrt{\frac{\epsilon_r \epsilon_0 k_b T}{2 N_A e^2 I}}$$



**Supplementary Figure-S2: Debye length calculations at various ionic concentrations of NaCl solution.** This figure shows the characteristic Debye length,  $\lambda_D$ , and its relation with ionic concentrations of the fluid. The Debye length would determine the length for which electrostatic force interactions will extend from the surface of the DLD pillar.

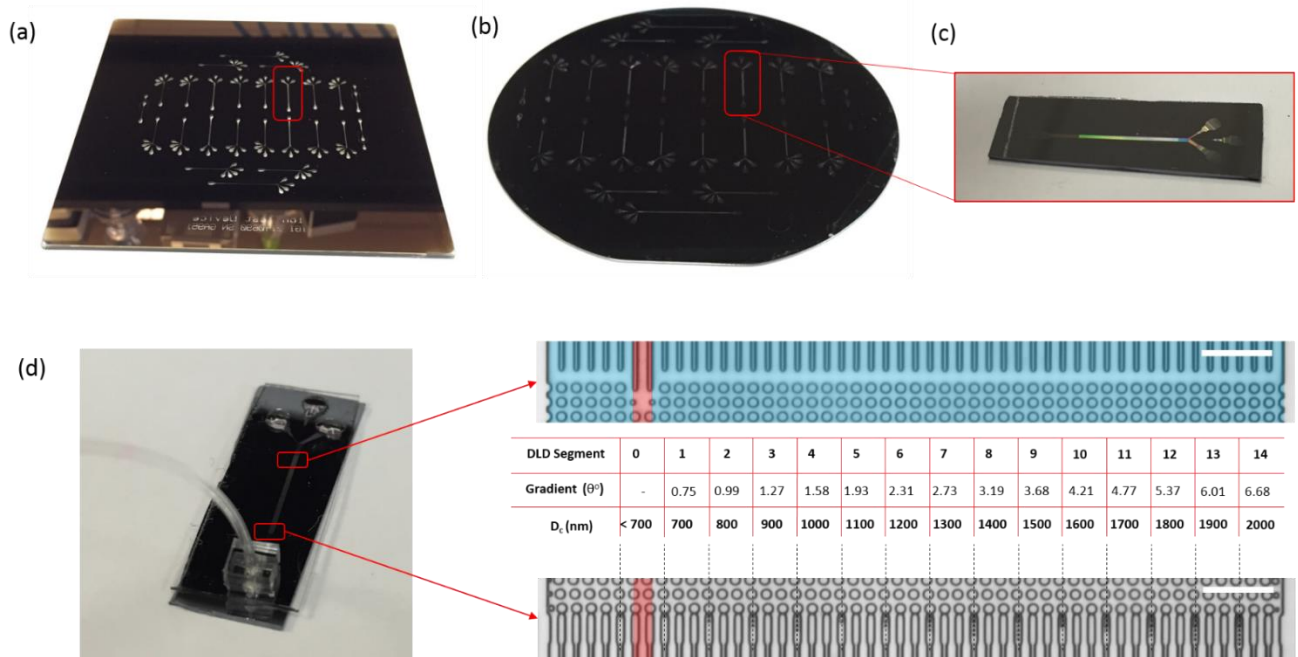
As ionic concentrations of NaCl of approximately  $10 \mu\text{M}$  correspond to a Debye length of  $\sim 100\text{nm}$ , pore sizes larger than  $500\text{nm}$  are generally not considered in nanoparticle separations.

### Supplementary Information 3: Fabrication Diagrams



**Supplementary Figure-S3: Fabrication diagrams of DLD device using standard lithography and deep reactive ion etching methods.** (a) A blank silicon wafer of 4" diameter is used as the substrate for DLD channels. AZ5214E positive photo resist is coated onto the surface by spinning the wafer at 4000 rpm for 60 seconds. (b) The coated resist is baked on a hot plate at 95°C for 1 min. The wafer is transferred onto a mask aligner where the glass chrome mask is used as a template for the DLD device. (c) The designs are transferred onto the photo-resist using a 365nm UV wavelength exposure. (d) The patterns emerge after developing in AZ developer diluted with DI water in a ratio of 1:1. (e) Deep reactive ion etching (DRIE) is used to etch away the exposed silicon substrate. Each cycle of the DRIE etches approximately 1  $\mu\text{m}$  in depth. 4 cycles were used to reach a depth of approximately 4  $\mu\text{m}$ . (f) After the channels were etched, the protective photoresist layer was removed and the silicon wafer was cleaned using Piranha solution. (g) To cover the silicon channels to complete the device, a thin PDMS layer of  $\sim 1\text{mm}$  is used to seal the channels. Two holes were punched into the device to fabricate sample reservoirs and tube insertion for sample extraction using syringe pumps.

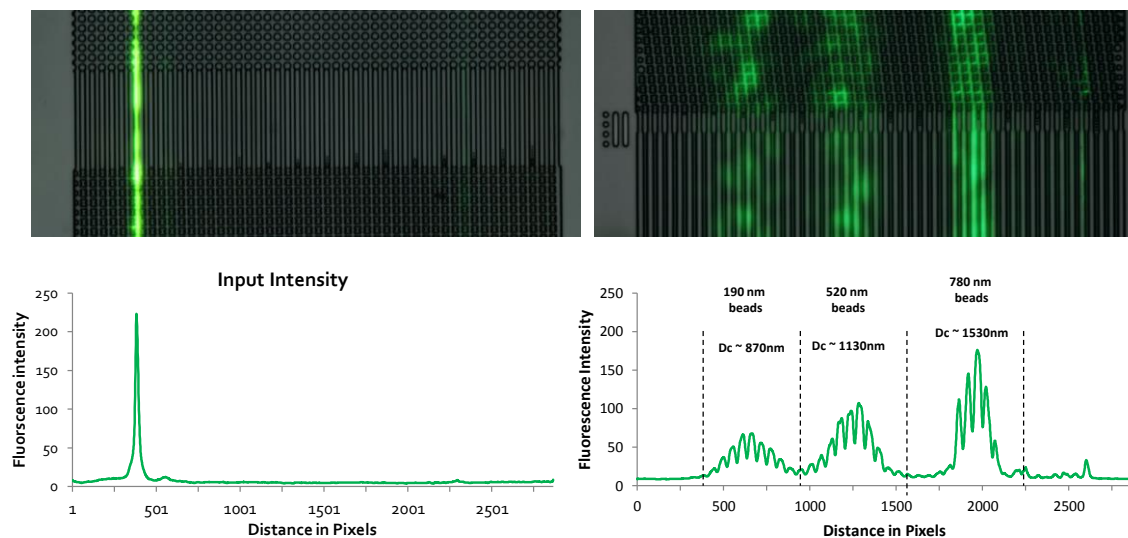
## Supplementary Information 4: Device Fabrication and Setup



**Supplementary Figure-S4: Device fabrication and setup.** (a) shows the mask used in the device fabrication. The fabricated device is shown in (b) where the channels and DLD patterns are etched into the silicon wafer. The diced silicon wafer is covered with PDMS to complete the setup shown in (d). Magnified images of the input and output can be seen in (d).

## Supplementary Information 5: Particle separation mixture

The predicted DLD separation model with electrostatic forces were tested using a particle mixture of 200nm, 500nm and 800nm particles in a DI water medium for which the particle separation output were shown as a fluorescence plot indicated in figure 6. The device used here is the same device shown in the main manuscript Fig S3.

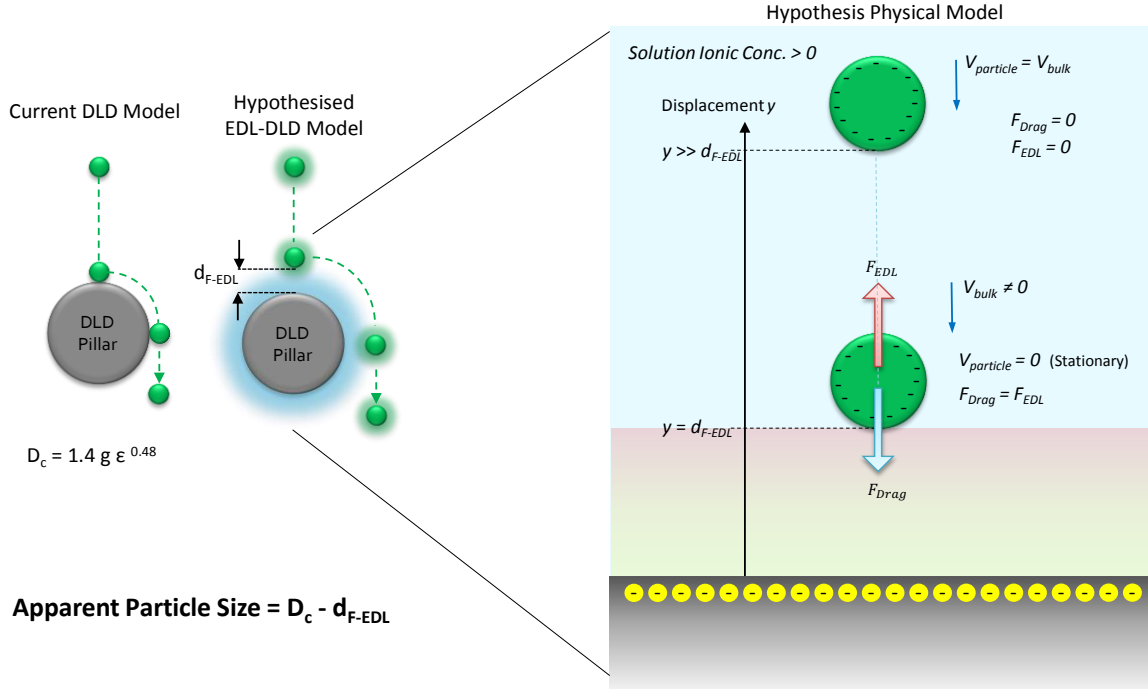


**Supplementary Figure-S5: Separation of a particle mixture in the DLD device.** A particle mixture comprising of 190nm, 520nm and 780nm were introduced into the input stream shown as a single stream of strong fluorescence intensity. The output stream shows three distinct fluorescence intensity spectrum of each particle size.

For a thin sample input stream, the output stream were separated into three distinct regions indicated by fluorescence signal curves for 190nm, 520nm and 780nm at DLD Dc of 870nm 1130nm and 1530nm respectively. With a pore-size DLD gap of 4000nm, 200nm particles were separated distinctly from the original sample input stream with an approximate enhancement of 670 nm. This is an enhancement of more than 300%. To enable 200nm particle separation of 4000-nm pore-size using standard DLD techniques in equation 1 requires a device of length 1 meter with a width of 1 mm. However, using the EDL enhanced DLD, we only require a 50 mm long device.

## Supplementary Information 6: Derivation of $d_{F-EDL}$

As the electrostatic force component is neglected in current microfluidic DLD models, we propose an EDL-DLD model which considers how electrostatic forces change the separation critical diameter of a DLD pillar array. The proposed model is depicted in Supplementary Figure-S4. where the apparent particles size in a DLD device has an added  $d_{F-EDL}$  component. The  $d_{F-EDL}$  measures the minimum displacement of the particle from the pillar surface due to electrostatic force interactions. This added displacement will enable the particles to appear bigger or smaller depending on the magnitude of  $d_{F-EDL}$ .



**Supplementary Figure-S6: Hypothesised EDL-DLD model for nano-particle separation.** The current DLD model is depicted to predict particle separation based on  $D_c = 1.4g\epsilon^{0.48}$ . The proposed model accounts for the electrostatic effects of particles and surface charge which is assumed to be dominant for nanoparticles. The electrostatic forces is balanced with the drag force at a distance  $d_{F-EDL}$  from the surface of the device. This distance will be accounted for in the apparent particle size for the DLD system.

To simplify the system, there are 4 main assumptions:

- (1) We assume that the size of the particle is much smaller than the size of the pillar such that we are calculating the forces of a sphere and a planar surface.
- (2) The charges on the sphere and surface are of the same sign such that they repel each other.
- (3) The velocity of the fluid is also assumed to be uniform at  $V_{bulk}$ .
- (4)  $d_{F-EDL}$  is large enough to neglect Van der Waals and hydration forces.

Based on the assumptions, the electrostatic force acting on a spherical particle and a charged surface can be approximated by:

$$F_{EDL} = \frac{2\pi\lambda_D R}{\epsilon_0 \epsilon} \left( (\sigma_p^2 + \sigma_s^2) e^{-2D/\lambda_D} + 2\sigma_p^2 \sigma_s^2 e^{-D/\lambda_D} \right) \quad (2)$$

Where the electrostatic force  $F_{EDL}$  is dependent on the Debye length ( $\lambda_D$ ), radius of particle ( $R$ ), electrical permittivity of the medium ( $\epsilon$ ) and free space ( $\epsilon_0$ ), distance of particle ( $D$ ) from the surface, the surface charge density of the particle ( $\sigma_p$ ) and surface ( $\sigma_s$ ). This equation is used by Butt to determine the electrostatic forces acting on a spherical tip in atomic force microscopy.<sup>3,4</sup> When the particle is at distances much larger than  $d_{F-EDL}$ , electrostatic force influence on the particle is zero and the particle is assumed to be sufficiently small to move with the bulk fluid in a laminar flow such that Stokes drag force is also zero. The Stokes drag force can be computed by force  $F_{Drag} = 6\pi\mu R V_{bulk}$  where the laminar flow drag force  $F_{Drag}$  experienced by a spherical particle is proportional to the relative velocity of the surrounding fluid  $V_{bulk}$ , its radius ( $R$ ) and the viscosity of the fluid ( $\mu$ ). Since the small particle is moving together with the bulk fluid ( $V_{particle} = V_{bulk}$ ), the drag force on the particle relative to surrounding medium is 0.

As the particle moves closer to the charged surface, it experiences an increasing repulsive electrostatic force which reduces the magnitude of its velocity relative to the planar surface. At some distance  $d_{F-EDL}$  from the surface, the electrostatic force sufficiently large such that it momentarily reduce that particle velocity to zero relative to the surface. At that distance  $d_{F-EDL}$ , the particle experiences the maximum drag force by the moving bulk fluid where  $F_{Drag} = F_{EDL}$ .

Hence by solving the force equations and rearranging the formula, we get

$$D = d_{F-EDL} = -\lambda_D \ln \left[ \frac{-\sigma_p^2 \sigma_s^2 + \sqrt{\sigma_p^4 \sigma_s^4 + \frac{(\sigma_p^2 + \sigma_s^2)^3 \mu \epsilon_0 \epsilon_r V_{bulk}}{\lambda_D}}}{\sigma_p^2 + \sigma_s^2} \right] \quad (3)$$

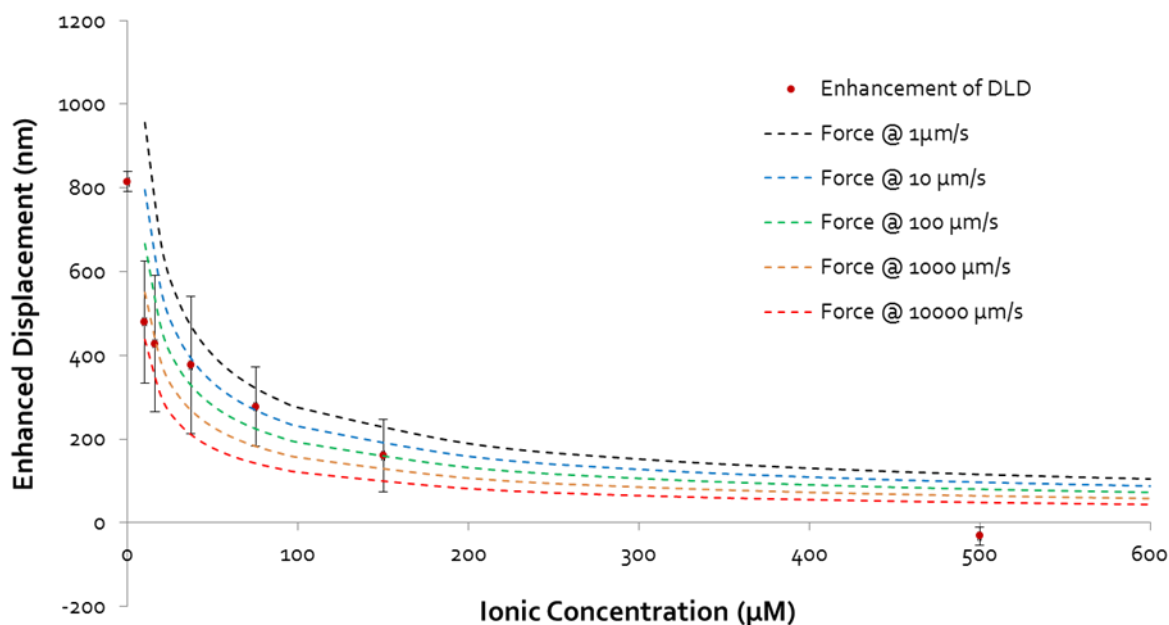
Where  $d_{F-EDL}$  is largely affected and proportional to  $\lambda_D$ , is independent of the particle radius and dependent on fluid velocity. Based on the proposed model,  $D_{APP} = D_p + d_{F-EDL}$ . Hence, for  $D_p \gg d_{F-EDL}$ , we can ignore electrostatic forces and determine the DLD specifications using the established empirical formula. For  $D_p$  smaller or slightly larger than  $d_{F-EDL}$ , electrostatic force interactions would significantly affect DLD separations. For instance, for a 50 nm particle, a 500 nm  $d_{F-EDL}$  would signify a 10 fold increase in size. Hence, accounting for ionic buffer effects is necessary for nano and even micron particle separations in DLD systems.

## Supplementary Information 7: Velocity plots of $d_{F-EDL}$

Ionic conc. of [Na+] ( $\mu\text{M}$ )	Average Critical Size Deviation from Theoretical DLD Calculations
0 (DI water)	+ 815 nm
10	+ 480 nm
16	+ 427 nm
37	+ 377 nm
75	+ 277 nm
150	+ 160 nm
500	- 32 nm
100000 (PBS)	- 263 nm

$$d_{F-EDL} = -\lambda_D \ln \left[ \frac{-\sigma_p^2 \sigma_s^2 + \sqrt{\sigma_p^4 \sigma_s^4 + \frac{(\sigma_p^2 + \sigma_s^2) 3\mu\epsilon_0 \epsilon_r V_{bulk}}{\lambda_D}}}{\sigma_p^2 + \sigma_s^2} \right]$$

EDL Force enhancement on current DLD model



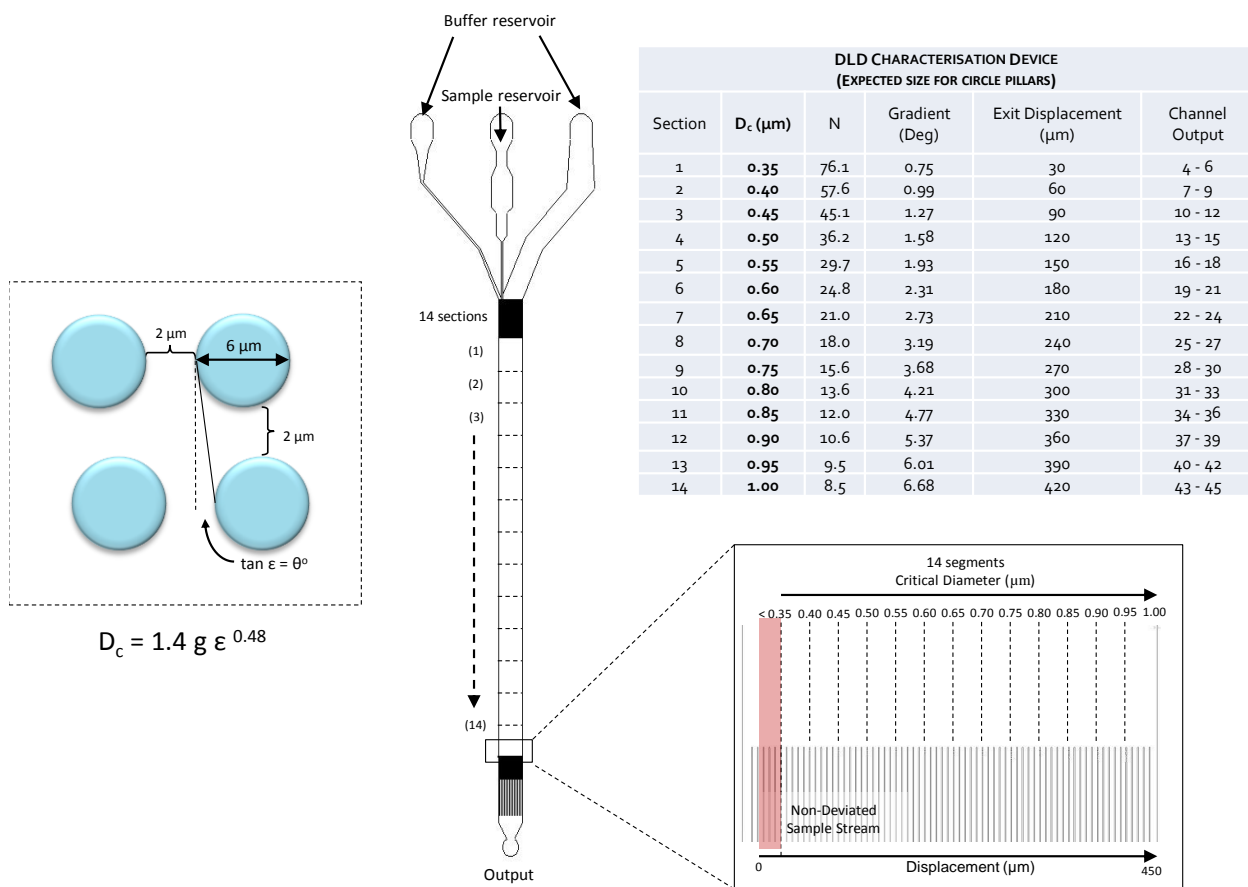
**Supplementary Figure-S7: Hypothesized EDL-DLD model for nano-particle separation.** The current DLD model is depicted to predict particle separation based on  $D_c = 1.4g\epsilon^{0.48}$ . The proposed model accounts for the electrostatic effects of particles and surface charge which is assumed to be dominant for nanoparticles. The electrostatic forces is balanced with the drag force at a distance  $d_{F-EDL}$  from the surface of the device. This distance will be accounted for in the apparent particle size for the DLD system.

The size deviations from theoretical DLD model were plotted against the ionic concentrations from 0 to 500  $\mu\text{M}$  in Supplementary Fig-S5 in comparison of the modelled  $d_{F-EDL}$  at different ionic concentrations and different velocity curves. Increasing the flow velocity reduces the enhanced displacement which is reasonable as the hydrodynamic forces on the particle are increased, a larger electrostatic force is required to oppose it corresponding to a position closer to the charged surface at a reduced  $d_{F-EDL}$ . Fig-S5 shows a lower and upper limit of practical flow velocities of microfluidic devices where the predicted electrostatic force enhance displacement seem to correlate with the experimental data for DLD effects.

Even at high velocities of 1cm per second in a microfluidic device, the  $d_{F-EDL}$  is still larger than Debye length approximations shown in Fig 4c in the main manuscript.

This shows the independency of particle size to electrostatic enhanced DLD systems. Hence it is predicted that the effects will drastically affect nanoparticle separations when size of nanoparticles can be many times smaller than  $d_{F-EDL}$ . Large particles will still experience the electrostatic interaction except that proportionally,  $d_{F-EDL}$  is smaller than say a 20  $\mu\text{m}$  particle. However, these effects is predicted to be still dominant for particles less than 5  $\mu\text{m}$  where low ionic solutions can affect particle separations efficiency by more than 10%.

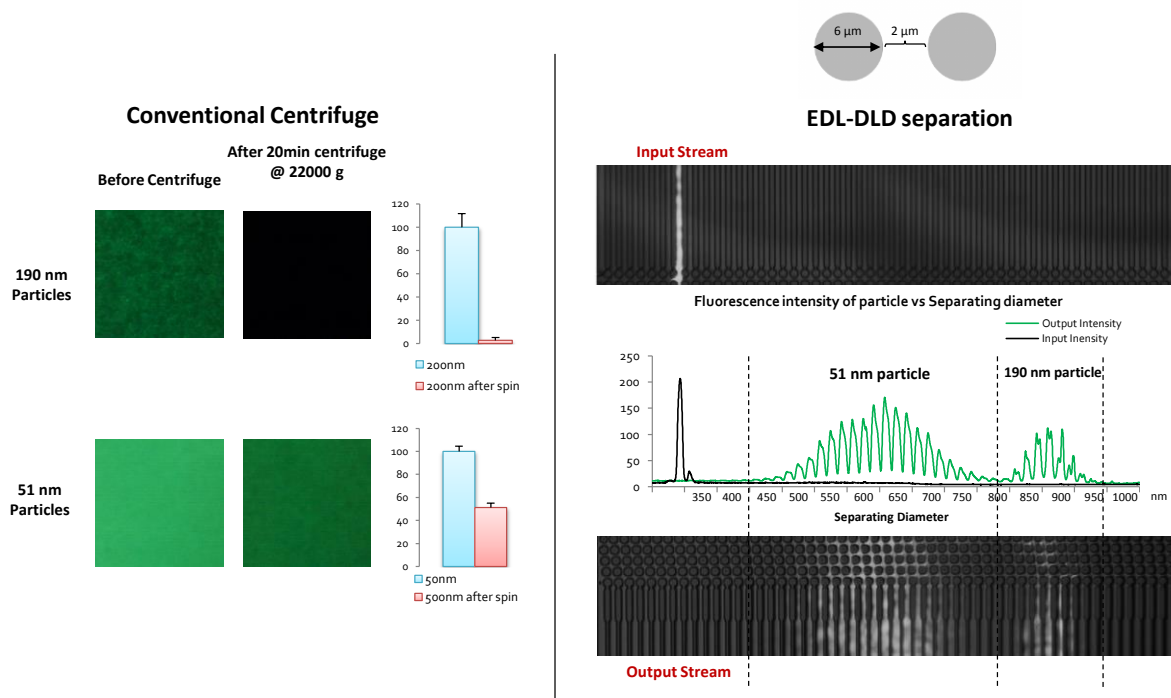
## Supplementary Information 8: Design parameters of 2.0 $\mu\text{m}$ gap DLD device



**Supplementary Figure-S8: Specifications of nanoparticle separator DLD device.** The specifications of DLD separation device is shown in this figure. Similarly, the device comprises of 14 segments and each segment consists of a pillar gradient array. The  $D_c$  of the device ranges from 350 nm to 1000nm. The gap between the pillars is reduced to 2  $\mu\text{m}$ .

Supplementary Fig-S6 depicts the nano-particle characterization device which is used to test 50 to 200 nm polystyrene bead separation. This device is fabricated in the same method as the DLD device shown in Figure 1 and as described in the fabrication methods in the main manuscript. Only the mask design for DLD gap size is different. The period between pillar to pillar has been reduced from 10  $\mu\text{m}$  to 8  $\mu\text{m}$ . Using this device, it is now possible to test the EDL-DLD model on nano-particle separation.

## Supplementary Information 9: Centrifugal techniques vs DLD device for nanoparticle separation



**Supplementary Figure-S9: Nanoparticle separation in an EDL-DLD enhanced device compared to conventional centrifuge method.** 51nm and 190nm particles were tested in the centrifuge system for separation of particle from the sample medium by spinning at 22000g in a centrifuge (a). The sample particle with the same concentration were tested in the DLD system and found to have a distinct separation between 51nm and 190nm particles with very little overlap in spectrum (b).

We compared the EDL-DLD particle separation to conventional centrifuge methods for the same nanoparticle separation. After 20 mins of centrifuge at 15000 RPM with 22000 g, the 190nm particle completely settled down while only approximately 50% of the 51nm particles settled down. Supplementary Fig S7 shows the reduction in fluorescence intensity of the supernatant after centrifuge which is used to determine the centrifuge efficiency. DLD microfluidic systems are continuous flow separators where immediate extraction of sample is possible resulting in multiple extraction while not compromising contamination of samples during pipetting processes. This makes microfluidic devices much more superior to current conventional centrifugal systems. Also, comparing with works from Arosio et al<sup>5</sup>, the separation is much more distinct while enabling real-time extraction of particles.



### **Supplementary Movie S1**

This movie shows a combined video of the output stream of separated particles ranging from 1000nm, 900nm, 800nm, 700nm and 600nm in DI water. The video streams were taken at 100fps and played back at 25 fps.

### **Supplementary Movie S2**

This Movie depicts the real-time separation of 500nm fluorescence particles with an overlaid channel to show the separating regions. The three segments coloured in red, green and blue show the final separating region of the particles after the ionic solutions were added.

## References

- 1 Zeming, K. K., Ranjan, S. & Zhang, Y. Rotational separation of non-spherical bioparticles using I-shaped pillar arrays in a microfluidic device. *Nat Commun* **4**, 1625, doi:[http://www.nature.com/ncomms/journal/v4/n3/supinfo/ncomms2653\\_S1.html](http://www.nature.com/ncomms/journal/v4/n3/supinfo/ncomms2653_S1.html) (2013).
- 2 Ranjan, S., Zeming, K. K., Jureen, R., Fisher, D. & Zhang, Y. DLD pillar shape design for efficient separation of spherical and non-spherical bioparticles. *Lab Chip* **14**, 4250-4262, doi:10.1039/c4lc00578c (2014).
- 3 Butt, H.-J. Measuring electrostatic, van der Waals, and hydration forces in electrolyte solutions with an atomic force microscope. *Biophys J* **60**, 1438-1444 (1991).
- 4 Butt, H.-J. Electrostatic interaction in atomic force microscopy. *Biophys J* **60**, 777-785 (1991).
- 5 Arosio, P., Müller, T., Mahadevan, L. & Knowles, T. P. J. Density-Gradient-Free Microfluidic Centrifugation for Analytical and Preparative Separation of Nanoparticles. *Nano Letters* **14**, 2365-2371, doi:10.1021/nl404771g (2014).